Proceedings of the Institute of Acoustics

FINITE ELEMENT MODELLING OF THE A.R.E. LOW FREQUENCY FLEXTENSIONAL TRANSDUCER

R.J. Brind

Admiralty Research Establishment, Portland, Dorset

INTRODUCTION

In the design of underwater sound projectors, a large volume displacement is required to produce a high acoustic output at low frequencies. Flextensional transducers achieve this by having a conventional stack driving a curved radiating surface at its flexural resonance. Over the past five years ARE(Portland) has had an interest in several types of flextensional transducer as sources for active sonar systems. A 350Hz low frequency flextensional prototype has been developed, manufactured and tested; the technology is the subject of a license agreement with DTE Ltd.

Conventional equivalent circuit methods can not be applied to these complex designs. The finite element method provides a practical means of modelling the flexural deformations and fluid loading effects. This paper describes finite element analyses performed using the PAFEC software available at ARE in support of the low frequency prototype development. A complete description of the analysis of the transducer will not be given here; rather points that bring out the capabilities and limitations of the finite element method will be emphasised.

CONSTRUCTION

Details of the construction and initial calibration of the first prototype are given by Bromfield [1]. The transducer consists of a GRP cylindrical shell 21mm thick with an elliptical cross section. Along the major axis plane lie three piezo-electric stacks joined together by a central nodal plate. The contact between the stack assembly and the shell is distributed by Aluminium inserts, see Fig 1. The shell is covered externally by a neoprene moulded boot which has a serrated surface over each end cross section. The end plates are held in place against this, to produce a water-tight seal and decoupling between the shell and the end plates.

The principle of operation of the transducer is that small longitudinal vibrations in the stacks give rise, because of the elliptical shape of the shell, to large flexural deformations at the minor axis. The result is a large volume displacement and, since the transducer is small compared to the wavelength of sound in water, the radiation of omnidirectional sound. The major and minor axis dimensions and the thickness of the shell determine the frequency of resonance.

The effect of external hydrostatic pressure is to extend the length of the stacks. This can lead to failure of the ceramic which is weak under tension. To overcome this a compressive pre-stress is introduced into the stacks during assembly of the transducer. The shell is deformed under a large minor axis load, the stacks are inserted and tapered wedges are used to take up the gap.

the shell from the end-plates.

The frequencies of the first few symmetric normal modes of the structure without the boot in air were calculated. The mode shape of the first mode for a 21mm shell is shown in Fig 5; the fundamental frequency is 673Hz . The calculation was repeated using the refined mesh and a result for the frequency of the fundamental mode of 656Hz obtained, a difference of 2.7% . The variation of the in-air resonant frequency with shell thickness is plotted in Fig 6.

In these diagrams, the displaced shapes are viewed from along the axis of the elliptical cylinder and a slight variation of the displacements of the shell at different axial positions is evident. The shape of the fundamental mode is made clearer in Figs 7 and 8. Fig 7 shows the displaced outline in solid lines, and the original outline in dashed lines, of the elements at an axial position mid way between the plane of symmetry in the centre of the transducer and the end-plate. Fig 8 shows in the same way the elements on the minor axis looking along the direction of the stacks from the inserts.

The displacements in all three modes are much greater on the minor axis than the major axis, confirming that a large volume change can be produced by a small change in the stack length. This amplification effect is due to the elliptical shape of the cross-section of the shell. In the fundamental mode the minor axis displacements vary little with axial position; in the higher modes however there is much more variation. In reality, the decoupling seal will have some restraining effect on the motion of the shell and result in a slight lowering of the natural frequencies. This effect will be greater in the higher modes.

Modes and frequency calculations were also performed for the structure with the boot included. The PAFEC calculations are apparently affected by numerical ill-conditioning caused by the great difference in stiffness between the GRP and the unrestrained rubber. The modes shapes must therefore be examined very carefully to check that the results are realistic. Increasing the number of master degrees of freedom generally improves the results. The PAFEC software selects these master degrees of freedom in the structure automatically, and uses them to reduce the number of degrees of freedom retained in the eigenfrequency calculation. Fig 9 shows the variation of the in-air resonant frequency with the boot included using 120 masters in the PAFEC calculation. The boot reduces the fundamental frequency by approximately 30Hz .

In-air admittance loop measurements on the prototype transducers indicated resonant frequencies of between 650Hz and 690Hz [1]. The finite element predictions for the booted transducer of 644Hz with the course mesh and 625Hz with the refined mesh are in reasonable agreement with the measurements.

During the development of the prototype transducer, it was noticed that the width of the inserts in contact with the shell had a significant effect on the resonant frequency. Originally the inserts occupied the whole of the internal volume of the elliptical cross section up the plane of the stack/insert boundary, as in Fig 10. The shell suffered local delamination damage at the sharp corner during the insertion of the stacks, and it was decided to profile the inserts to a shape shown in Fig 5. The shells manufactured with the profiled inserts were more compliant, and they would be expected to lead to a

lower frequency transducer. A finite element calculation was performed with the original inserts and the course mesh, and a resonant frequency of 710Hz obtained with a mode shape as shown in Fig 10. Thus, a 5.3% lowering of the resonant frequency is predicted to have occurred as a result of the minor change in the shape of the inserts.

IN-WATER RESONANT FREQUENCY CALCULATIONS

The loading of the external volume of water on the transducer was modelled using PAFEC 24620 and 24610 fluid-loading patches. These are based on the Doubly Asymptotic Approximation (DAA), which is an approximation exact at high and low frequencies. In the mid-range an impedance due to the fluid is calculated at each point on the surface by interpolating between the two ends of the frequency spectrum. There are several variants of the DAA depending on the number of terms at high and low frequencies reproduced by the approximation. The variants currently implemented in PAFEC are an added mass option and DAA2C [4].

In the current implementation the fluid-loading patches can be applied to a structure with a closed external surface or a structure bounded by three orthogonal planes of symmetry. In order that this should be the case for our model of the flextensional transducer, the rubber seal and the end-plates must be included in the mesh. The seal was modelled using brick elements with the material properties used previously for the external boot. The 30mm stainless steel end-plates were modelled using PAFEC 44210 and 44110 facet shell elements. The end-plate and the edge of the seal in contact with it were restrained, to avoid deformations of the rubber dominating the deformations of the shell.

The frequencies of the first few symmetric normal modes of the structure in water were calculated using the DAA added mass option. The mode shapes of the first mode for a 21mm shell is shown in Fig 11. The fundamental frequency was 335Hz . The variation of in-water resonant frequencies with shell thickness is shown in Fig 12.

The prototype transducers were found to have a measured free-field resonant frequency of between 330Hz and 340Hz . Thus the agreement between predictions and measurements is excellent.

STACK PRE-STRESS

Effect of Ambient Pressure

A PAFEC analysis was performed to calculate the effect of a 2MPa hydrostatic pressure on the surface of the transducer, which corresponds to a depth of 200m . The stress distribution in the ceramic of the stacks is approximately uniform and is shown in Fig 13. The stress contour plot displays the principal stress with largest absolute value, and the contour values have been chosen to span the narrow range of stresses in the ceramic. Ambient pressure of 2MPa produces a tensile stress of approximately 85MPa in the stacks. The direction of this principal stress lies very nearly along the axis of the stack.

Measurements [1] on the prototype transducer under hydrostatic pressure indicate

a 89MPa reduction in ceramic stress with a 2MPa increase in ambient pressure after correcting for non-linear behaviour at low hydrostatic pressures. Thus the agreement between measurements and finite element predictions is very good.

Interference Fit between Stack and Shell

A PAFEC analysis was performed to find the pre-stress that would be produced in the ceramic by an interference fit between the stack and the shell. The interference fit was simulated in the PAFEC model using the thermal stress capability. The temperature is imagined to have increased to a high value, and the coefficients of thermal expansion of all parts of the transducer are set to zero except the longitudinal coefficient of thermal expansion of the ceramic. To allow for this anisotropic thermal expansion, the ceramic was modelled with PAFEC 37115 orthotropic elements but the elastic moduli used were equivalent to the isotropic values. Fig 14 shows the stress distribution in the ceramic, again exaggerated. An interference fit of 0.15mm per half stack produces a compressive pre-stress of approximately 4.5MPa in a direction very nearly along the axis of the stack. As long as the deformations are not great, the behaviour of the transducer under this imagined thermal loading is linear. Hence, an interference fit of 2.8mm per half stack is sufficient to give a pre-stress of 85MPa and by the preceding ambient pressure analysis a depth capability of 200m at zero drive voltage. The depth capability at non-zero voltages during operation will be less than this because of alternating stresses set up in the ceramic.

STACK INSERTION

It is necessary to predict the load necessary to open the shell sufficiently to achieve the interference fit, and to verify that the strength limits of the shell are not exceeded. A thorough series of shell deformation measurements were taken by the manufacturer on the production shells [5]. They were deformed using the external loading press designed for stack insertion. For a minor axis load of 23.5tonne typical semi-major and semi-minor axis displacements were 0.95mm and 8.3mm respectively.

PAFEC analyses were performed on the shell/insert combination using the refined mesh. The minor axis load was applied as a 3.2MPa pressure over the external surface of the finite element bricks next to the minor axis, i.e. over an area 0.1468m by 0.5m . The component of force in the downwards direction is 23.5tonne . The semi-major and semi-minor axis displacements were predicted to be 2.9mm and 14mm respectively. A contour diagram on the maximum tensile principal stress on the side of the shell/insert combination is shown in Fig 15.

It is evident that the measured minor-axis deformations is about half that predicted and the measured major-axis deformation only about one third. The shell is bonded to the inserts through the winding process during manufacture but they are also bolted together as a safety measure. The inserts are observed to move slightly relative to the shell when the shell is deformed. This would be expected to reduce the observed major axis displacement under minor axis loading.

The difference between the measured and predicted displacements has not yet been

explained. Displacements measured in this test configuration are the only displacement data available to validate the finite element analysis. It was suspected that the Young's modulus quoted by the manufacturer was too low, but when a higher value was used to reduce the predicted displacements the predicted resonant frequencies increased. Interestingly, the predicted stresses were broadly their previous values, indicating that the shell acted to distribute the applied load whatever the displacements required in the shell to achieve this. There was a possibility that the minor axis load was not applied uniformly across the area supposed. PAFEC analyses were performed applying the load in an area concentrated at the centre of the transducer, but the predicted displacements were little changed.

The quoted flexural strength and inter-laminar shear strength (ILSS) of the unidirectional E glass composite, which was the eventual choice for the production shells, was 1010MPa and 70MPa respectively. From Fig 15 it is clear that the flexural strength is not exceeded under this minor axis loading condition.

Fig 16 shows the distribution of tangential traction acting across laminations on the side surface of the shell under 23.5tonne minor axis loading. The stress component shown is sigxy where x is an axis tangential to the elliptical cross section and y is perpendicular to it. The contour plot was obtained using PIGS by selecting a small subset of elements and plotting directional stresses relative to axes rotated about the z axis by the appropiate angle for that set of elements. Because of the difficulty of entering a long sequence of commands from the keyboard without error, the commands were put in a file and PIGS run from this. An averaged/unaveraged option exists for the contour plotting of stress distributions. Unaveraged stresses are calculated at each node for every element that includes it in its topology, whereas averaged stresses are the mean of these. A good test for the adequacy of a mesh for modelling a particular stress distribution is to examine the unaveraged stresses for gross discontinuities between elements. By this criterion the refined mesh referred to earlier was good enough to model the flexural principal stresses but was unacceptable for the shear stresses. Fig 16 was obtained with a further refined mesh.

The maximum tangential traction acting across laminations is approximately 45MPa and occurs in the centre of the shell thickness at the edge; it is zero on the top and bottom surface of the shell as it must be on physical grounds since no loads are applied. The shear stress in the middle of the transducer length is approximately 20MPa . Early shells survived stack insertion but later shells, which were manufactured under less stringent supervision and were stored in damp conditions, failed by catastrophic delamination. When the failed shells were cut up, the cracks were found in the centre of the shell thickness on the minor axis. The PAFEC results for the stress distribution are in rough agreement with predictions made by AERE Harwell [6], using the classical theory of elasticity for the bending of bars. This work also showed that the inter-laminar shear strength (ILSS) depended on the volume of the specimen under test, in that a large volume would be more likely to have a critical flaw. For a complete transducer an ILSS of 51MPa is quoted, indicating that there is perhaps an inadequate margin of safety above the maximum calculated shear stress of 45MPa .

CONCLUSIONS

Finite element modelling undertaken in support of the development of the ARE 350Hz flextensional transducer has been described. The in-air and in-water behaviour has been analysed using two meshes, one with about half the spacing of nodes of the other.

Predictions of the in-air fundamental frequency were in reasonable agreement with measured values. The model ignored the seal and end-plates, whereas the resonant frequency of the transducer decreased slightly when the end-plates were attached. Numerical problems were encountered in the PAFEC calculations when modelling the external rubber boot, and particular care was required in interpretation of the results. Piezo-electric elements are available in PAFEC but here the ceramic was modelled with an equivalent isotropic elastic material as the appropiate boundary condition on the electrical degrees of freedom (voltages) is that they are clamped.

Predictions for the in-water fundamental frequencies were made using the PAFEC fluid-loading elements and were in excellent agreement with the observed values. The fluid-loading elements model the effect of an exterior fluid on a surface and are based on the Doubly Asymptotic Approximation. This approximation has been found elsewhere [4] to predict the position of the resonances in the frequency domain accurately through the added mass effect of the water, but found not to predict the magnitude of the radiative damping around resonance correctly. Thus the source level and bandwidth can not be calculated reliably with the PAFEC software presently available. However work is in hand at ARE and under contract at PAFEC to couple the Helmholtz Integral Equation method for the fluid domain to the finite element package for the structure. This should enable accurate source level and bandwidth to be determined.

Although not used here, piezo-electric elements will be required in the future for enforced harmonic motion calculations which would enable admittance loops and absolute vibration levels to be obtained. For these calculations, accurate methods for modelling radiative damping and internal material and electric damping would need to be developed.

The depth capability of the transducer has also been analysed using the finite element method. The predicted reduction in stack pre-stress, due to the external hydrostatic pressure corresponding to a depth of 200m , was in excellent agreement with that observed in the prototype transducer. The interference fit required to achieve this pre-stress was also determined. It was shown that a 23.5tonne minor axis load was needed to deform the shell by this amount. The shear stresses predicted by PAFEC to arise from this stack insertion load, are uncomfortably close to the inter-laminar shear strength. In the assembly of the transducers a minor axis load of 23.5tonne was found to be sufficient to achieve a depth capability of 200m at zero drive voltage, but the displacements on the major and minor axes were reported to be only about one half those predicted by the PAFEC analysis. Unfortunately this discrepancy has not yet been resolved.

FINITE ELEMENT MODELLING OF A FLEXTENSIONAL TRANSDUCER

REFERENCES

[1] Bromfield G. "The ARE 350Hz flextensional transducer." ARE unpublished report, April 1987.

[2] PAFEC Data Preparation User Manual 6.1, PAFEC Ltd, Strelley, Nottingham NG8 6PE.

[3] Brind R J. "Finite element modelling of the barrel stave projector." ARE unpublished report, September 1987.

[4] Macey P C. Ph.D. Thesis, University of Nottingham, January 1988.

[5] Raine C. "Development of flextensional projector shells." BAJ Ltd Contract Report (unpublished), February 1986.

[6] McLaren J R. "Development of fabrication technology for flextensional transducers." AERE Harwell Contract Report (unpublished), June 1988.

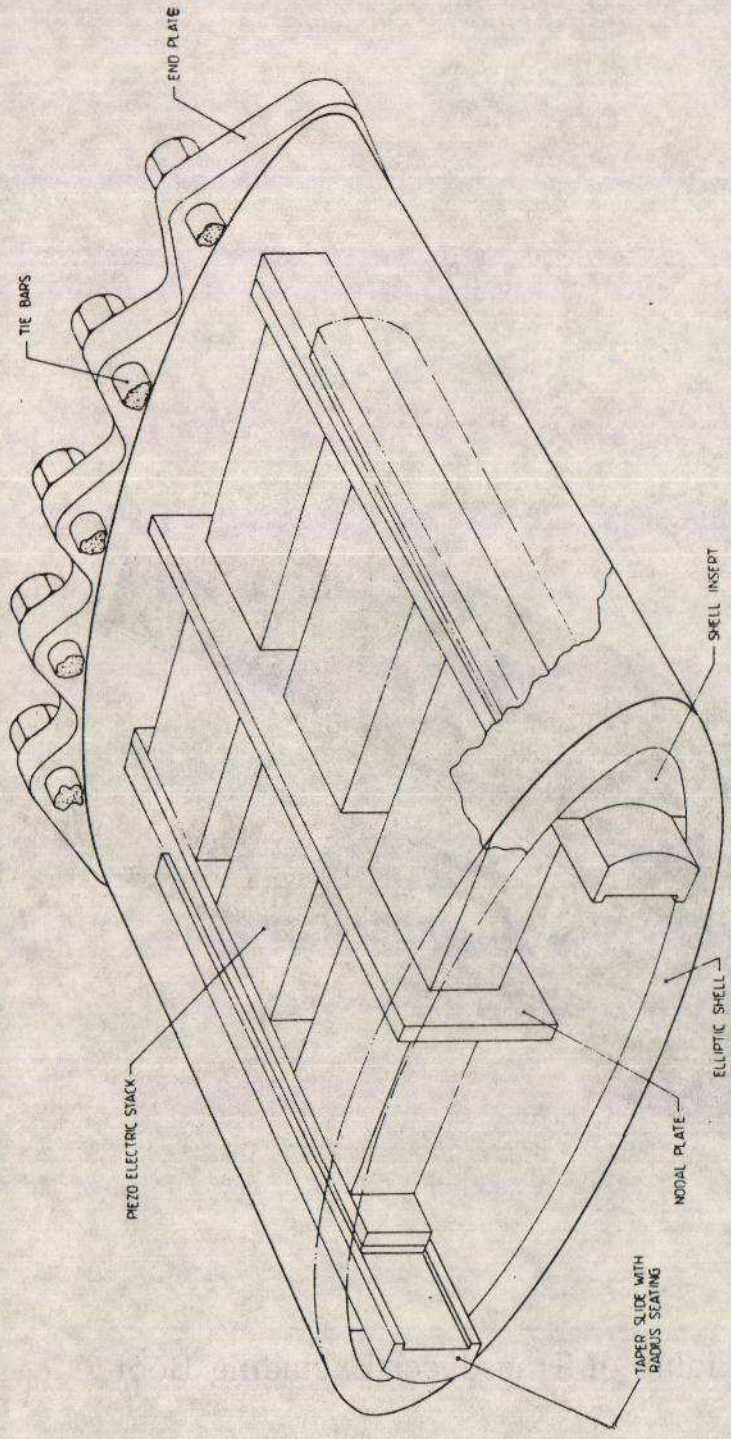

Fig 1: Construction of the Flextensional Transducer

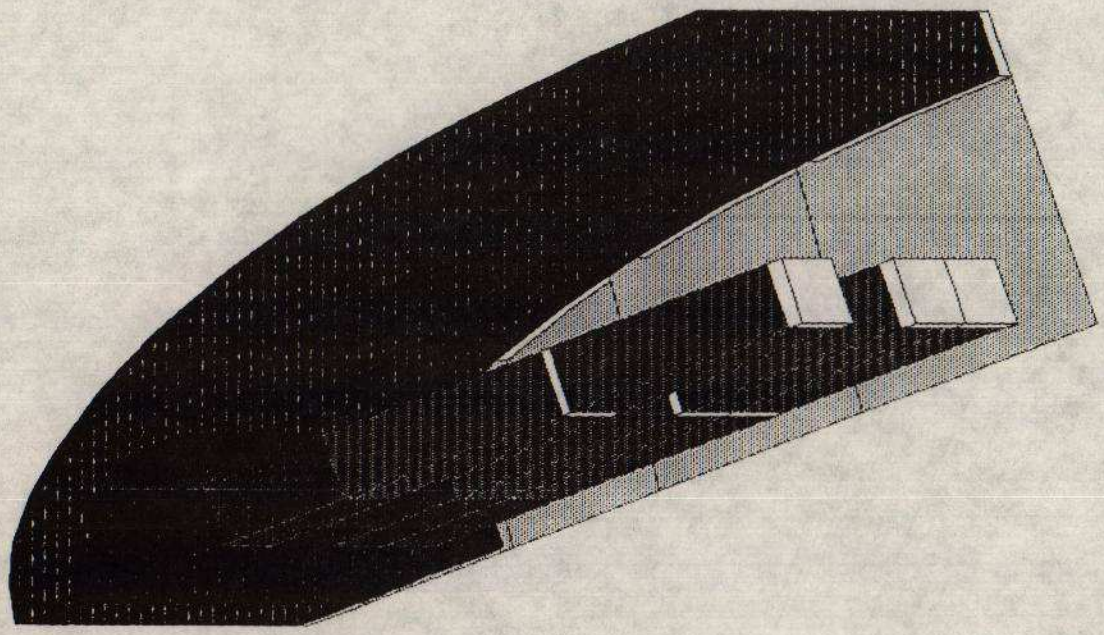

Fig 2: Model of One Eighth of Transducer Excluding Boot

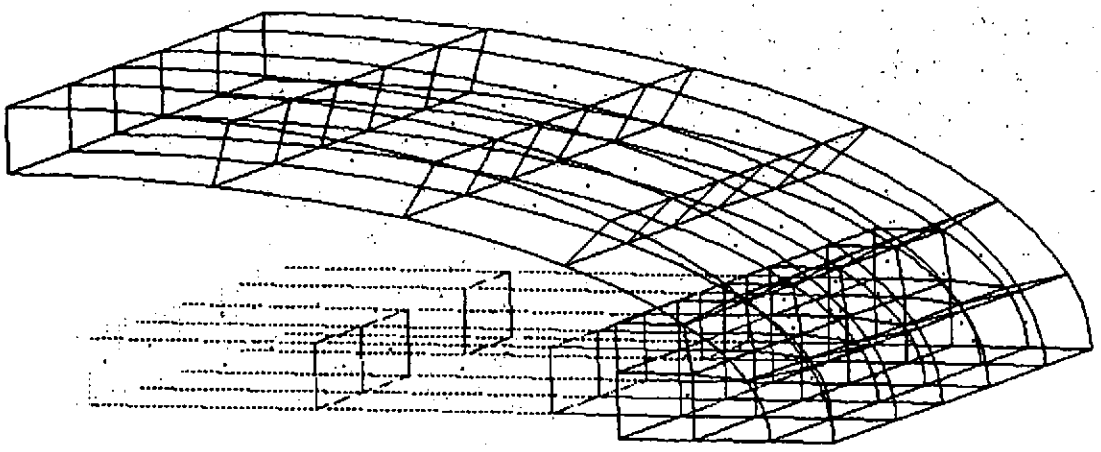

Fig 3: Course Finite Element Mesh: 937 Nodes

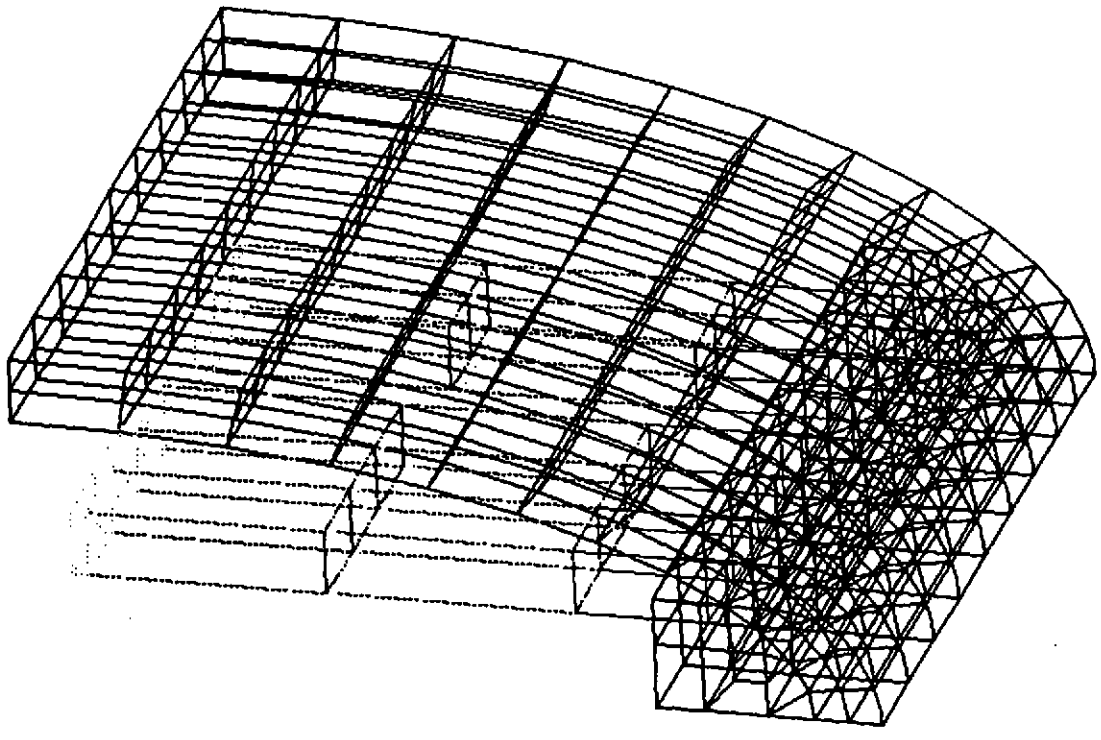

Fig 4: Refined Finite Element Mesh: 2089 Nodes

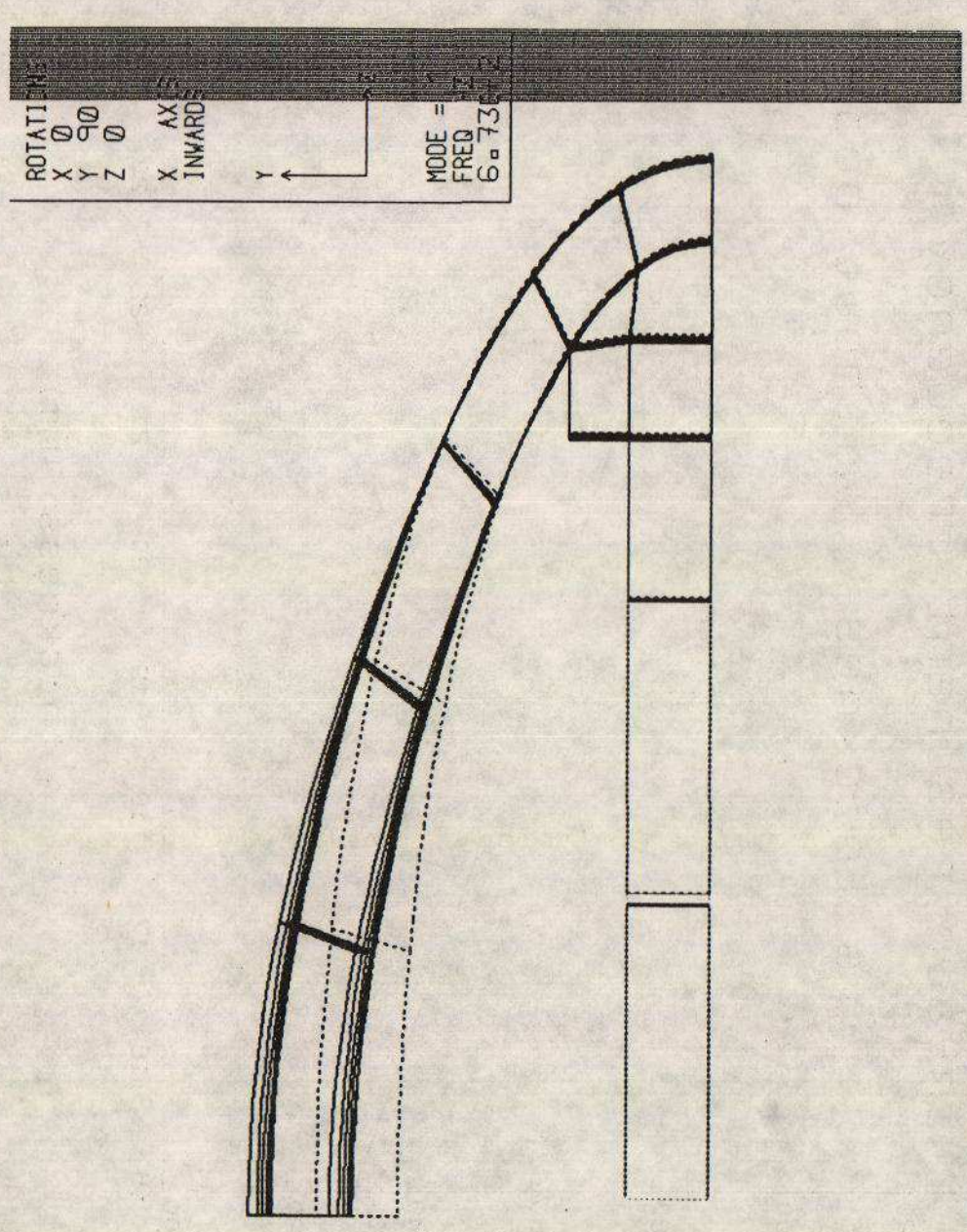

Fig 5: Mode Shape of First In-Air Natural Frequency

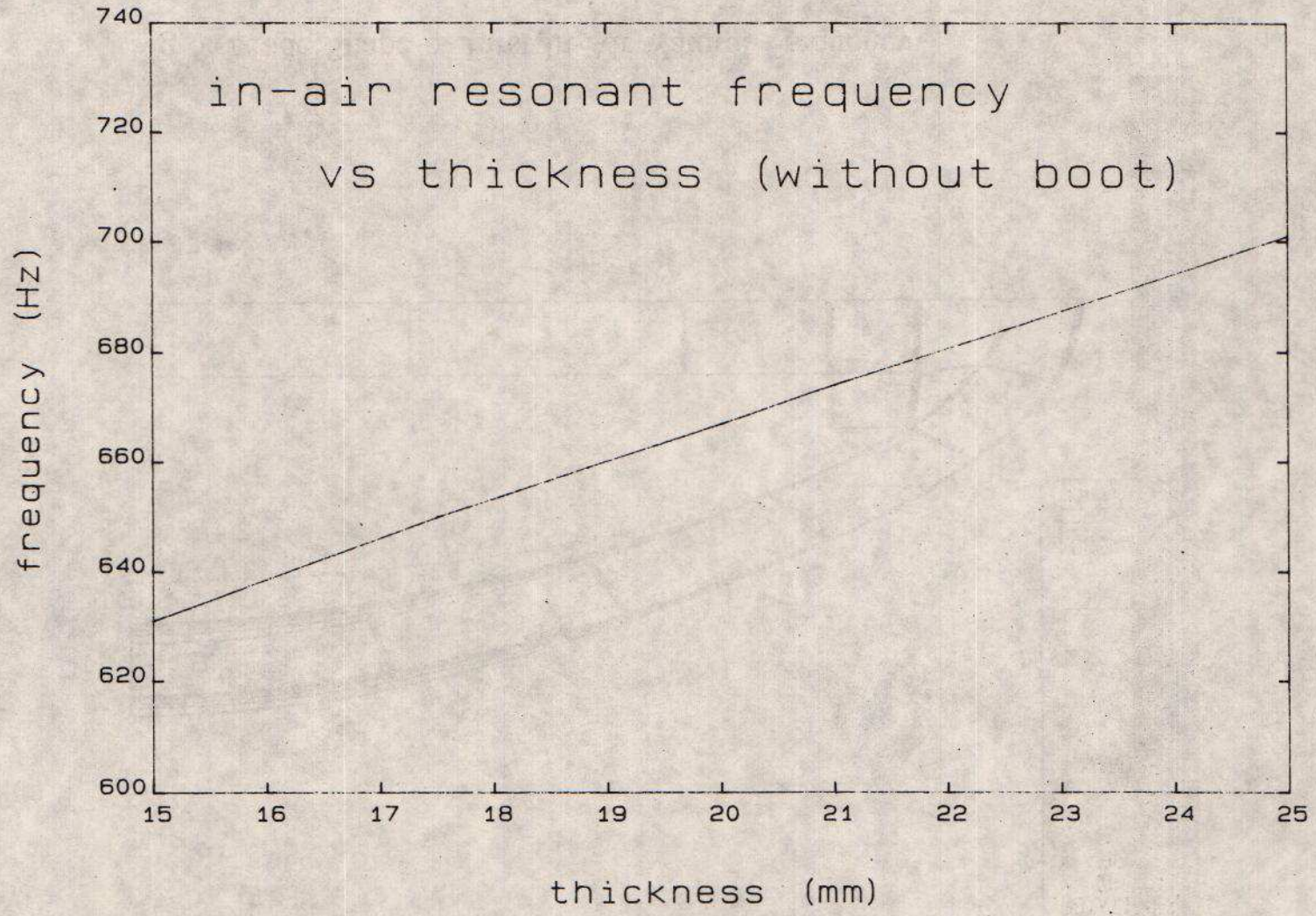

Fig 6: In-Air Fundamental Frequency vs Shell Thickness

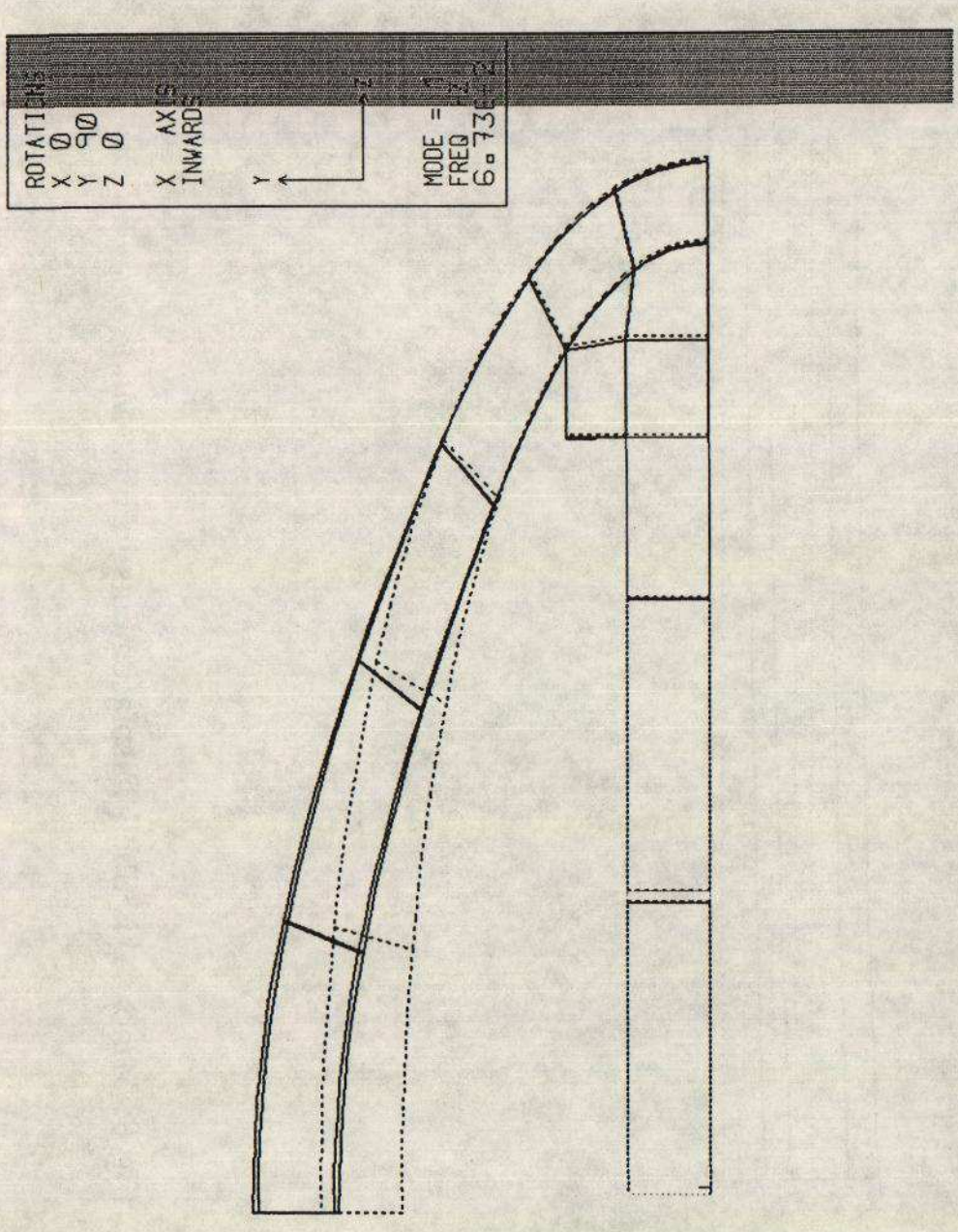

Fig 7: Displaced Shell Profile in First Mode

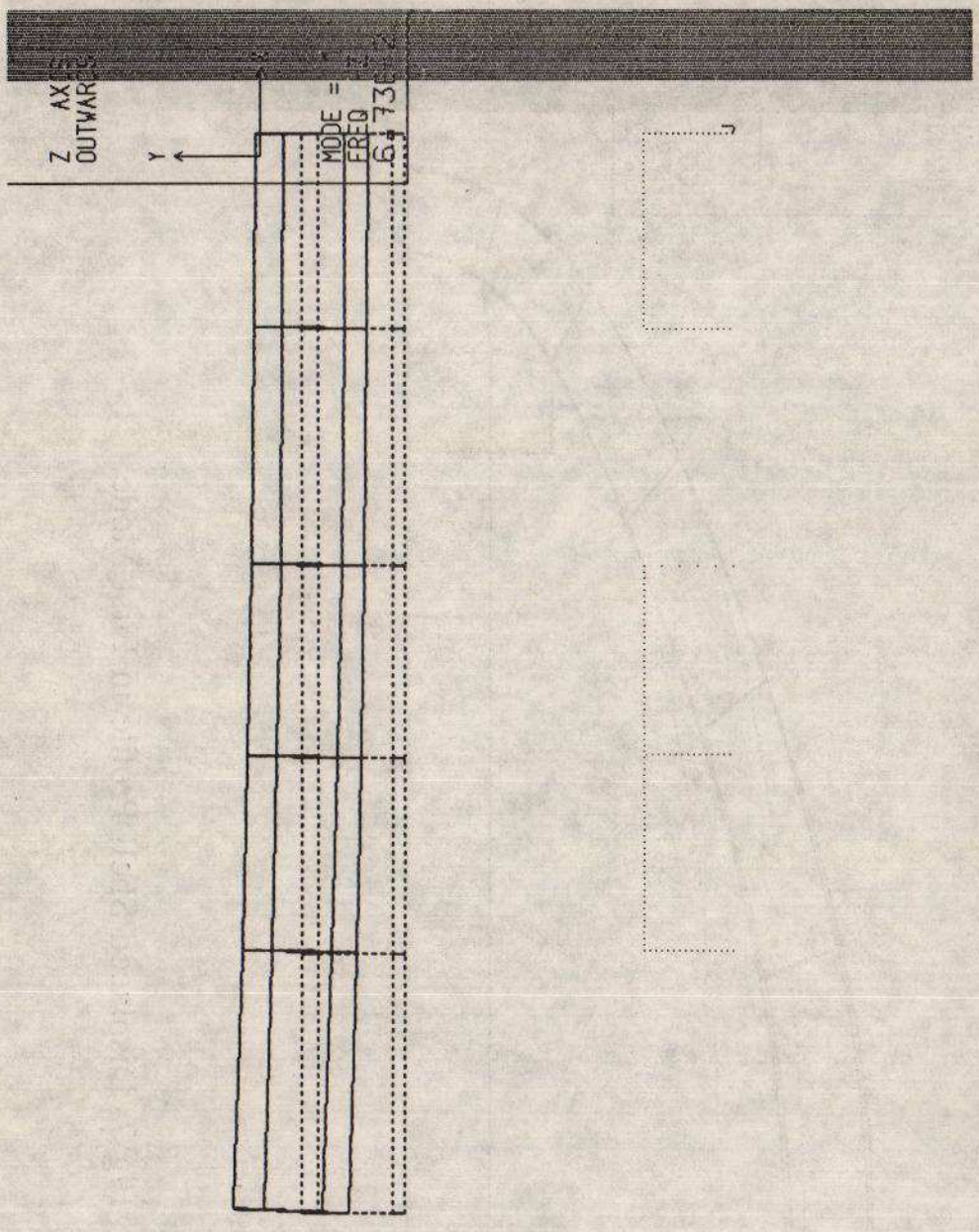

Fig 8: Minor Axis Shell Displacements in First Mode

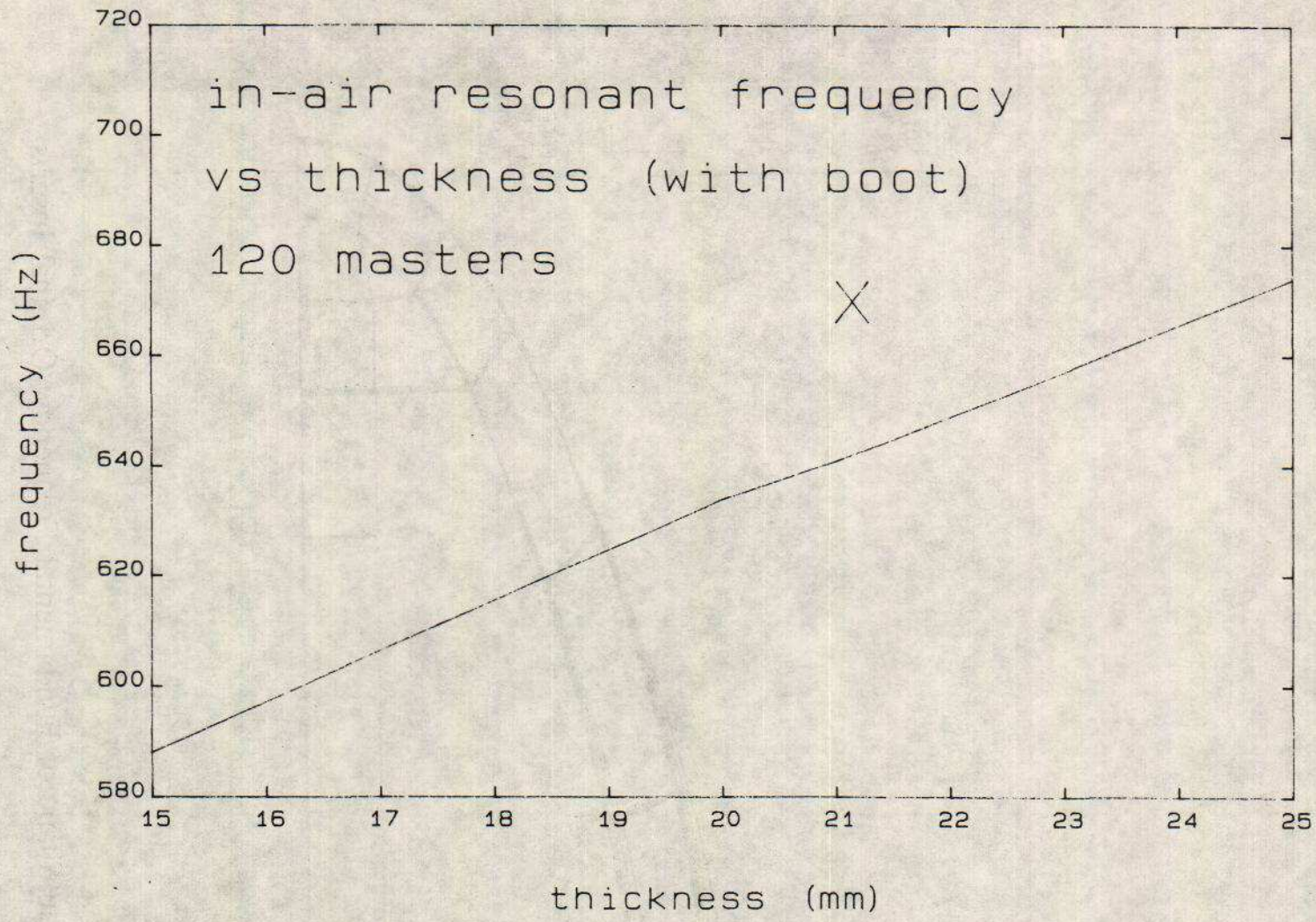

Fig 9: In-Air Frequency vs Shell Thickness: with Boot

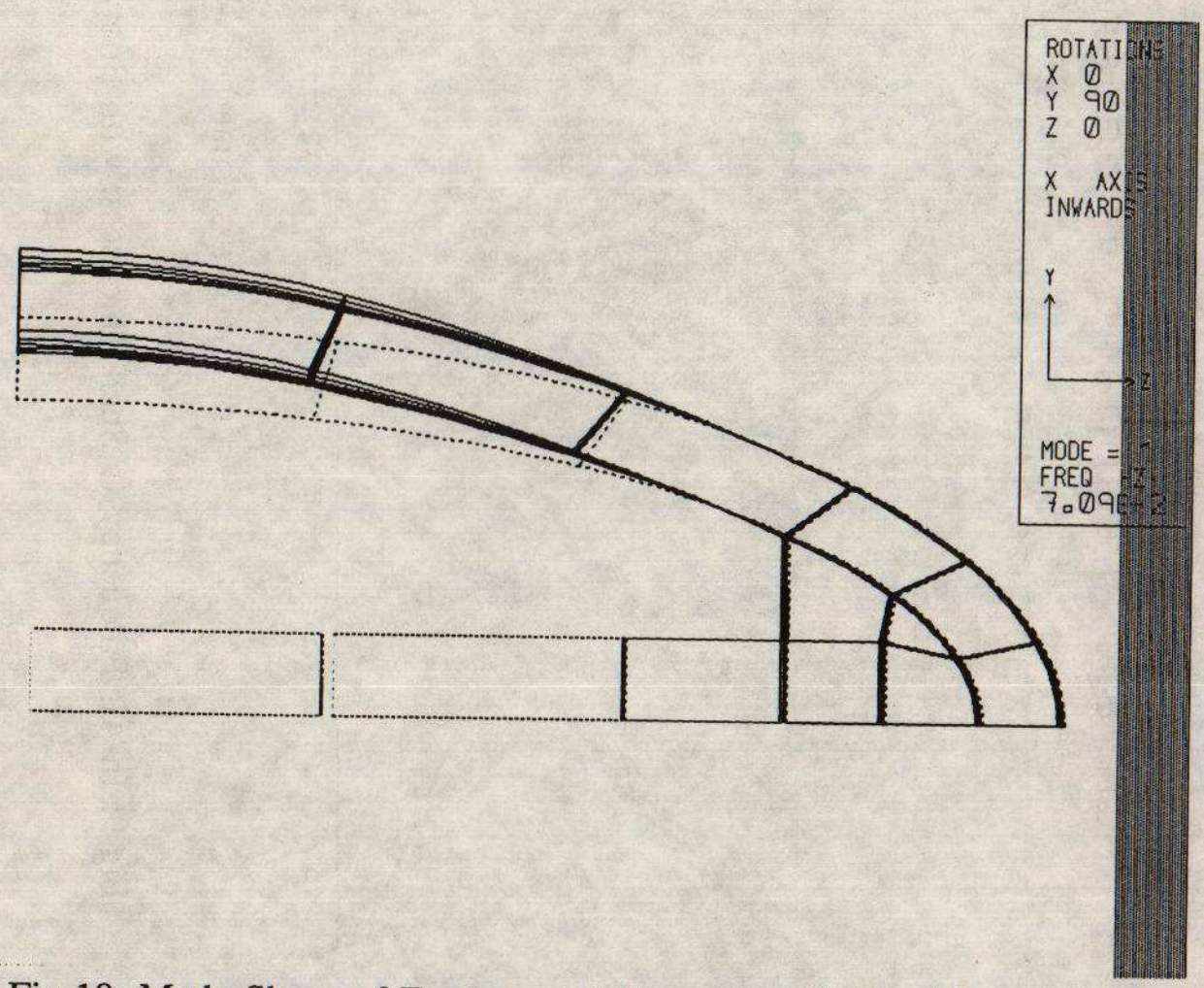

Fig 10: Mode Shape of Fundamental Frequency: Original Inserts

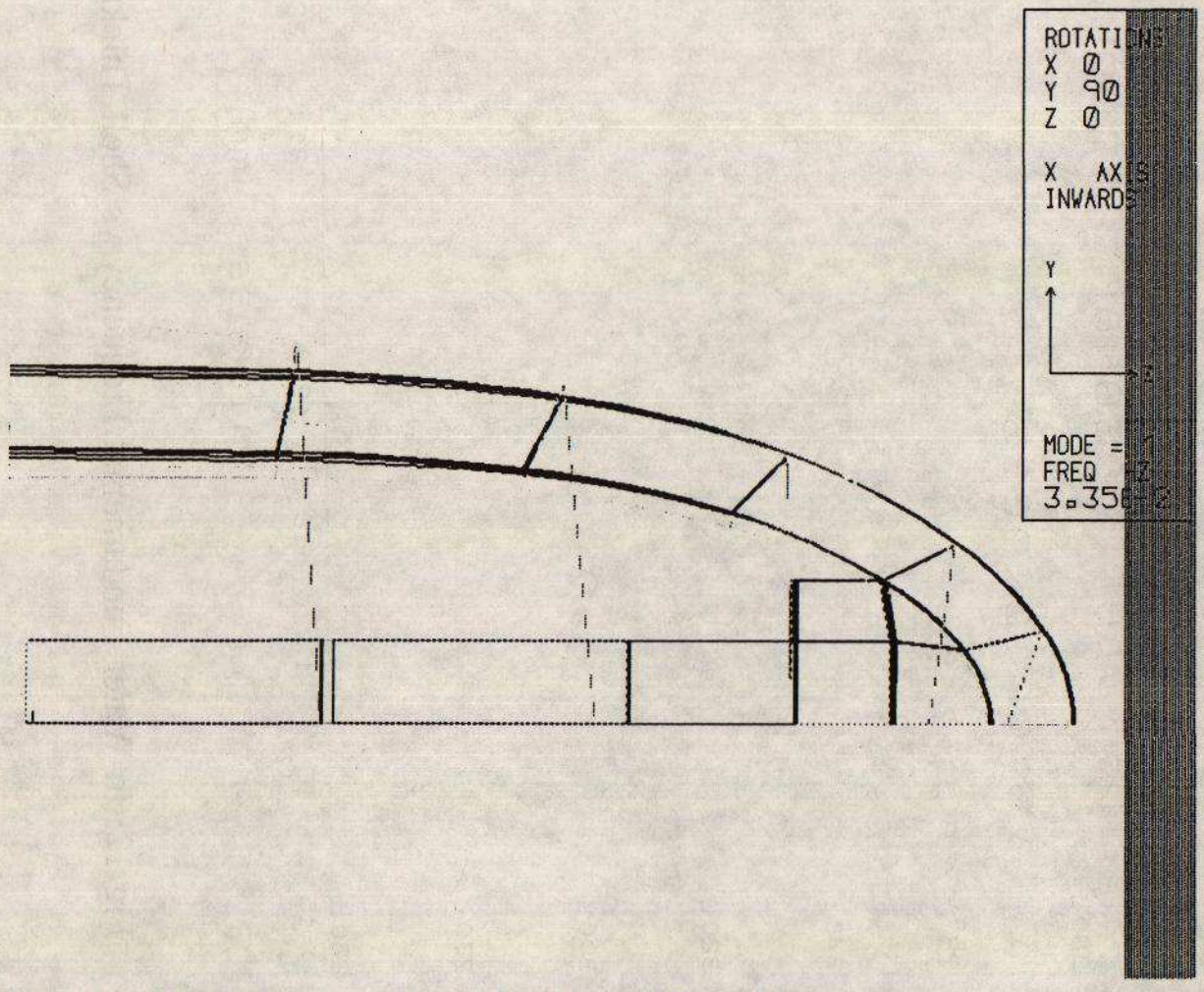

Fig 11: Mode Shape of First In-Water Natural Frequency

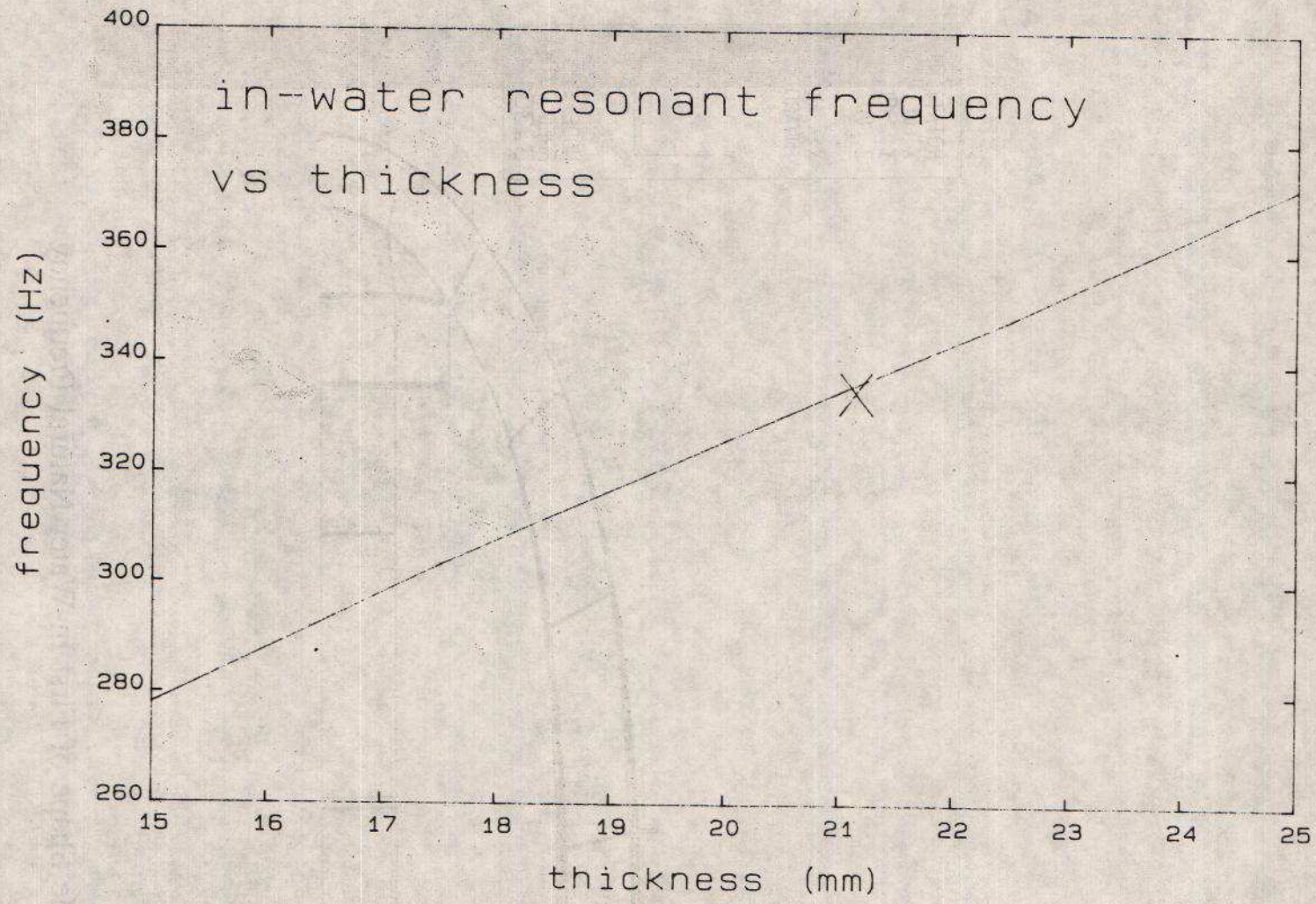

Fig 12: In-Water Fundamental Frequency vs Shell Thickness

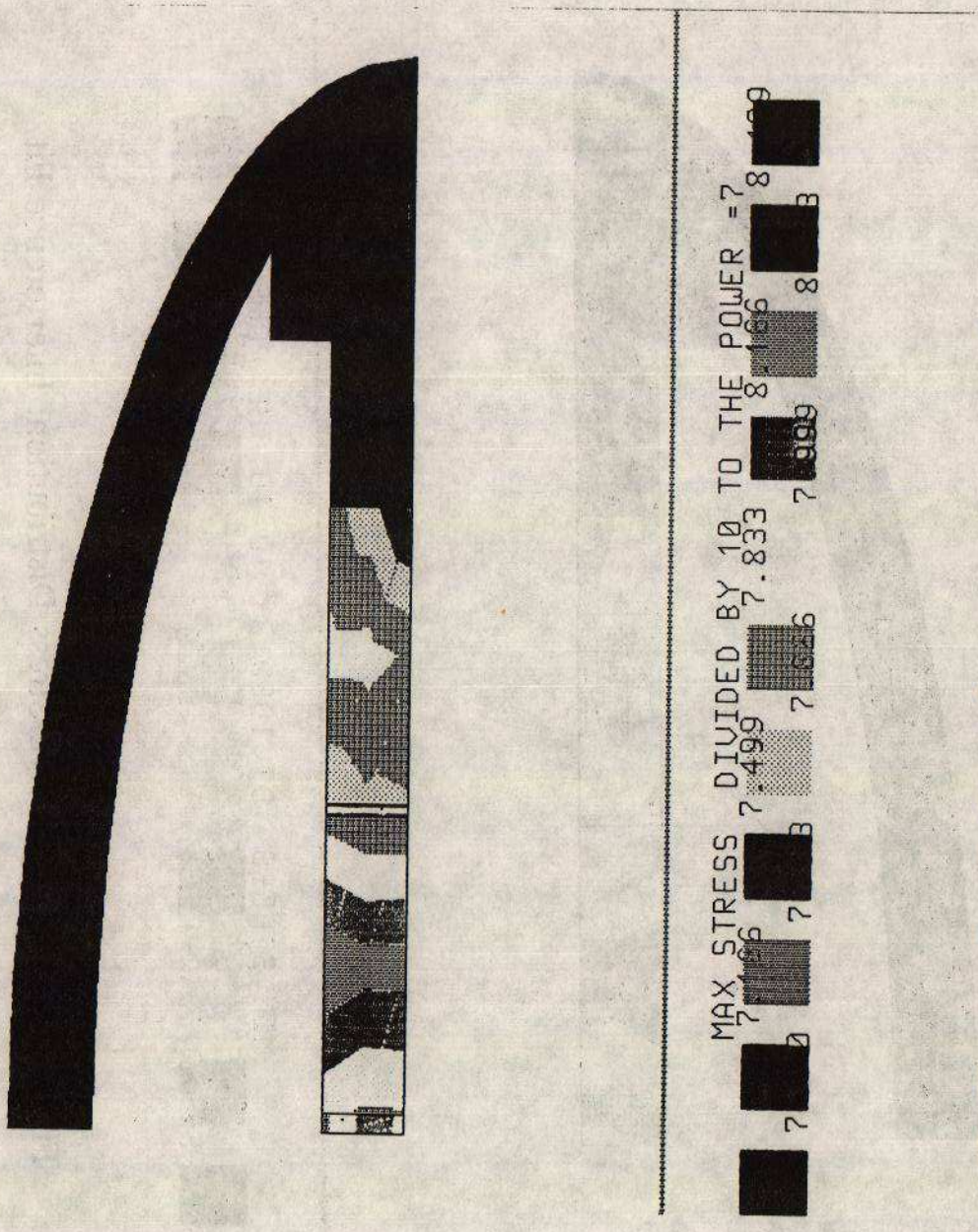

Fig 13: Max Tensile Stress Distribution: Ambient Pressure

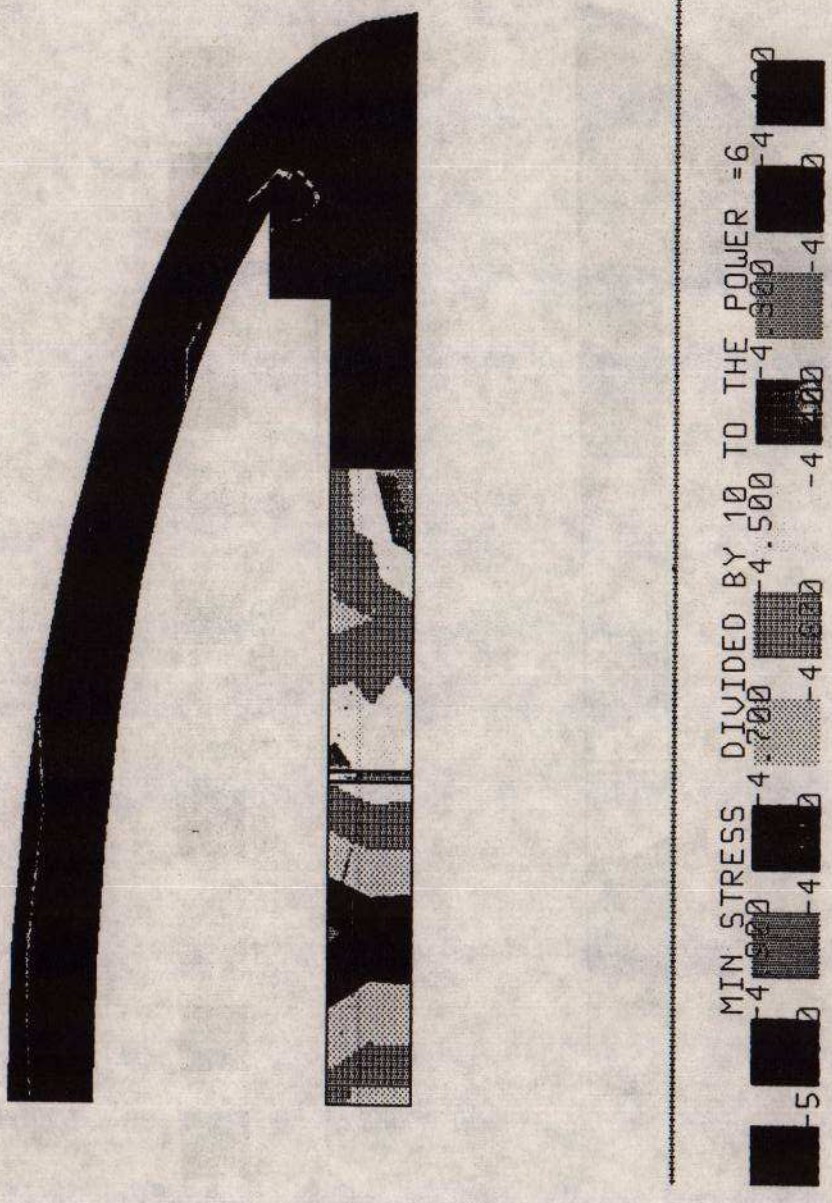

Fig 14: Max Compressive Stress Distribution: Interference Fit

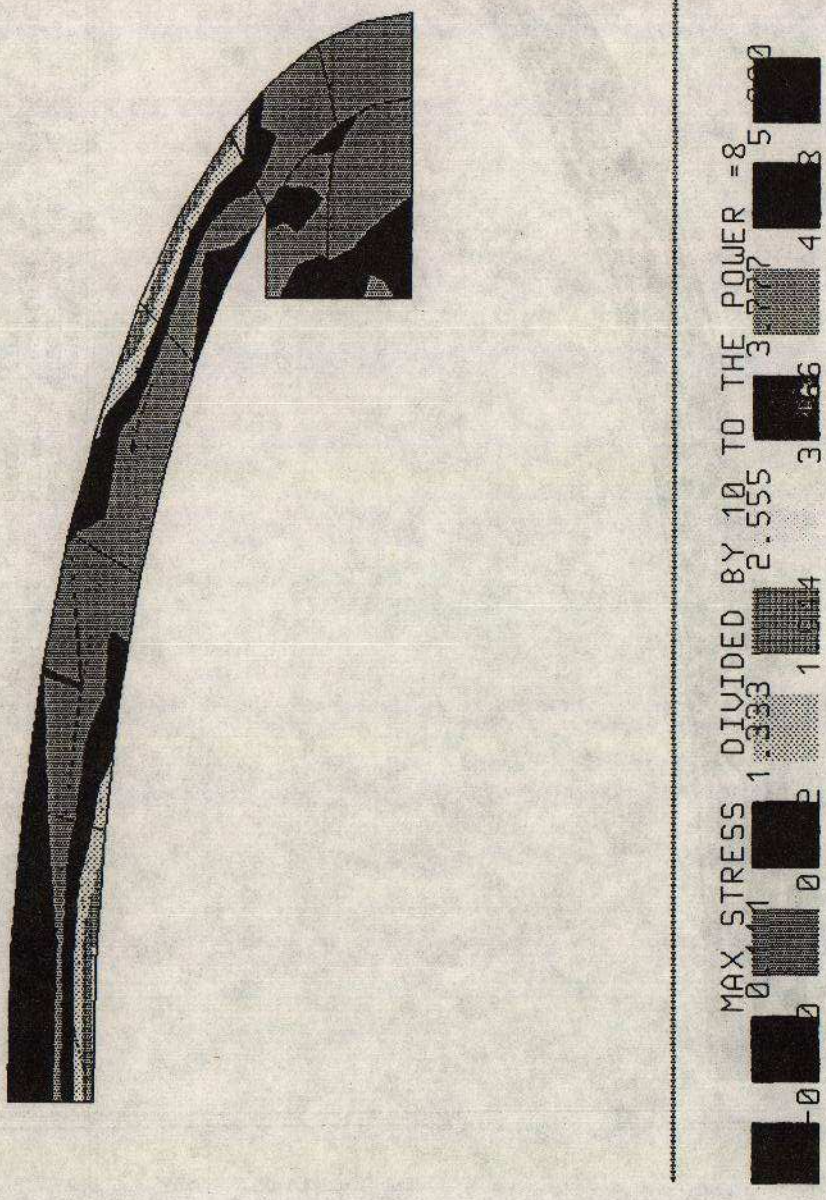

Fig 15: Max Tensile Stress Distribution: Stack Insertion

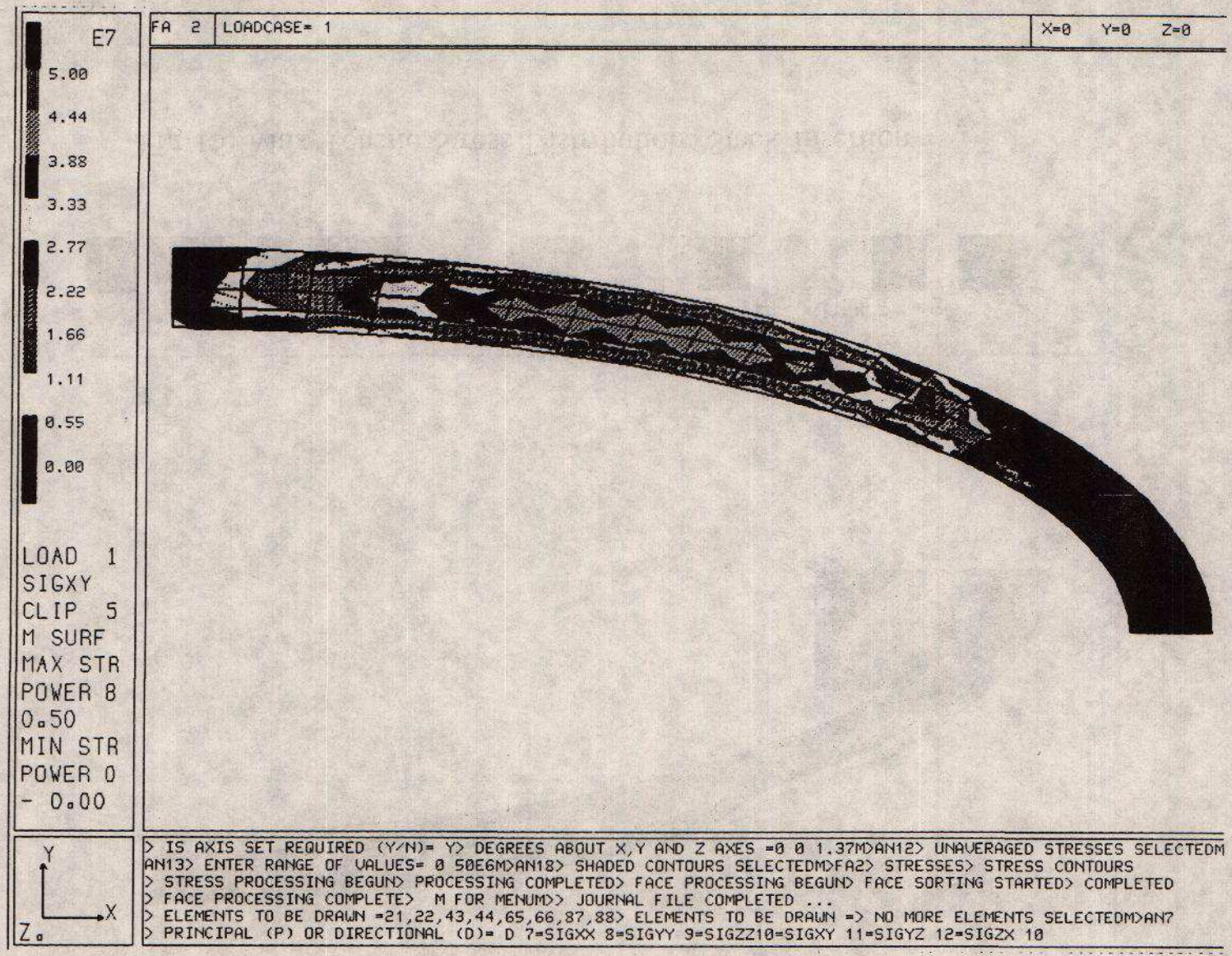

Fig 16: Distribution of Shear Stress: Stack Insertion